Research Article Vol. 4, No. 3 / 15 March 2021 / OSA Continuum 822

Transitions intensities and cross-sections of Tb^{3+} ions in $YAl_3(BO_3)_4$ crystal

Maxim Demesh,[1,*] Konstantin Gorbachenya,[1] Viktor Kisel,[1] Elena Volkova,[1,2] Viktor Maltsev,[2] Elizaveta Koporulina,[2,3] Elena Dunina,[4] Alexey Kornienko,[4] Ludmila Fomicheva,[5] and Nikolay Kuleshov[1]

[1] *Center for Optical Materials and Technologies, Belarusian National Technical University, Nezalezhnasti ave. 65, 220013, Minsk, Belarus*
[2] *Department of Crystallography and Crystal Chemistry, Lomonosov Moscow State University, 119991 GSP-2 Moscow, Russia*
[3] *Melnikov Research Institute of Comprehensive Exploitation of Mineral Resources, Russian Academy of Sciences, Moscow, Russia*
[4] *Vitebsk State Technological University, 72 Moskovskaya Ave., Vitebsk, 210035, Belarus*
[5] *Belarusian State University of Informatics and Radioelectronics, 6 Brovki Str., Minsk, 220013, Belarus*
[*] *demesh87@gmail.com*

Abstract: A Tb^{3+}:YAB crystal was grown using a high-temperature solution growth on dipped seeds technique. Polarized ground state absorption and fluorescence spectra from the $^5D_4$ level, as well as a fluorescence decay curves of $^5D_4$ and $^5D_3$ levels, were recorded at room temperature. Radiative properties such as emission probabilities, branching ratios, and radiative lifetime were investigated within the theory of *4f-4f* transition intensity in the case of the intermediate configuration interaction.

1. Introduction

Nowadays trivalent terbium doped materials are used not only as Faraday rotators [1] and green emitting phosphors [2], but as successful gain media for visible solid-state lasers [3–5]. Up to this time efficient laser operation was obtained only in the family of Tb-doped fluorides. Fluoride crystals possess the large bandgap energy and the weak crystal field strength that make them favorable for the visible laser operation [3]. But the low absorption and stimulated emission cross sections in the visible ($\sim 10^{-22}$ cm^2) is the main drawback of these crystals. To overcome this problem researches have been tried to find the suitable host among oxide crystals: aluminates [6], tungstates [7–8], phosphates [9]. Several papers regarding the common luminescent and absorption properties, as well as the crystal field analysis of Tb:$YAl_3(BO_3)_4$ [10] and $TbAl_3(BO_3)_4$ [11–12] were reported in the past. However, important properties regarding the applicability of Tb-doped borate crystals as laser materials have been not studied.

This work is devoted to the laser-related spectroscopic properties of Tb^{3+}-doped $YAl_3(BO_3)_4$ (Tb:YAB) for the visible optical application. The main advantage of oxyorthoborates is the low crystal field depression (CFD) of about 18000 ± 1000 cm^{-1} [13] among oxide crystals.

2. Experimental

Tb:YAB single crystals were grown by dipping seeded high-temperature solution growth method. Based on the earlier results, a complex flux of the $K_2Mo_3O_{10} - Y_2O_3/Tb_2O_3 - B_2O_3$ composition was used to grow such crystals [14]. Growth of Tb:YAB bulk crystal was performed in a resistively heated furnace. The temperature was monitored using a Proterm-100 precision temperature controller with a set of Pt/Pt–Rh thermocouples (S - calibration). The temperature in the working

#418643 https://doi.org/10.1364/OSAC.418643
Journal © 2021 Received 12 Jan 2021; revised 5 Feb 2021; accepted 8 Feb 2021; published 18 Feb 2021

OSA CONTINUUM

zone of the furnace was maintained with stability of ± 0.1°C. The initial load was prepared by stoichiometric mixtures of the rare earth, aluminium and boron oxides of 99.9% purity. The terbium concentration in the mixture was 35 at.%. $K_2Mo_3O_{10}$ was presynthesized by reacting potassium molybdate and molybdenum oxide at 650°C according to the scheme:

$$K_2\,MoO_4 \;+\; 2MoO_3 \rightarrow K_2\,Mo_3\,O_{10}$$

Starting chemicals were carefully mixed, grounded, and then the growth charge was loaded into 150-ml platinum crucibles and heated to 1130°C. The resulting melt was homogenized at this temperature within 24 h. Then, using the test seed method, the saturation temperature of the high temperature solution was determined, which was estimated to be 1058°C. Next, the melt was slowly cooled with rate from 1 to 1.5°/day. The growth process was completed at the temperature of 992°C. After that, the grown crystal was removed from the furnace and washed off from flux in a hydrochloric acid.

Identification of Tb:YAB crystal was carried out using ICCD database. Unit cell parameters were calculated from X-ray powder diffraction (XRPD) patterns using UnitCell software [15] for the hexagonal system (space group R32). XRPD set was collected using a computer-controlled ADP-3 powder diffractometer (Co K-α radiation cource, λ = 1.7903 Å; 2θ range – 6-80°). The composition and homogeneity of Tb:YAB crystal were studied using an analytical scanning electron microscope Leo 1420 VP with an INCA350 energy dispersive spectrometer. The analysis was performed on two adjacent well-developed as-grown faces of trigonal prisms and a polished cut plane perpendicular to the elongation of the crystal. The distribution coefficient of terbium (K_d) was defined as $K_d = C_{cryst} / C_{diss}$, where C_{cryst} is the Tb content measured in the crystal and C_{diss} is the nominal concentration, i.e. the concentration of Tb in the starting mixture.

For the spectroscopic measurements, the cut and polished sample with thickness of 3 mm and 1 mm were used. Polarized transmission spectra of the Tb:YAB were recorded in a Cary 5000 (VARIAN) spectrophotometer. In the visible and UV regions the spectral bandwidth (SBW) was set to 0.01-0.02 nm, and in the near infrared (NIR) region it was 0.1 nm. The fluorescence spectra were recorded under laser diode excitation at 488 nm. The fluorescence emission was collected on the input slit of MDR 23 monochromator with the SBW of 0.1 nm. The signal was detected with a C5460-01 APD module (Hamamatsu) associated with a SR830 Stanford lock-in amplifier. A gray body light source with a color temperature of 2900 K was used to correct the measured spectra with respect to the detector response, grating efficiency and other optical element`s influence.

The decay curve of the upper $^5D_4$ manifold was registered under pulsed excitation at 485 nm from an optical parametric oscillator LT-2214 (LOTIS TII). The fluorescence emission at 540 nm was imaged onto the entrance slit of a monochromator MDR-12. The signal was detected by a Hamamatsu photodetector C5460 connected to an oscilloscope Tektronix TDS-3052B.

3. Results and discussion

As a result, Tb:YAB single crystal with high optical quality with mass of 2.909 g and size of 15×8×8 mm has been grown. Observed morphology differs from that common for huntite-type borates. The grown crystal shown in Fig. 1 has been faceted by a combination of pinacoid (0001), two hexagonal prisms $(11\bar{2}0)$ and $(2\bar{1}\bar{1}0)$, three rhombohedron faces $(10\bar{1}1)$, $(40\bar{4}1)$ and $(02\bar{2}1)$. XRPD studies of Tb-doped YAB crystal confirmed that it exhibits *R32* space group (Fig. 2). Unit cell parameters of Tb:YAB single crystals obtained by least-squares refinement are as follows a = b = 9.3154(2) Å, c = 7.2814(5) Å, V = 547.202(3) Å^3. The investigations of Tb:YAB composition reveal that the Tb/Y ratio in the crystal obtained almost fully corresponds to the ratio in the starting flux melt and does not change during the growth process. This indicates that the solubility of end-members of the examined solid solution is comparable. The distribution coefficient of terbium is closed to the unit and estimated as 0.95-0.97 for all crystallographic

OSA CONTINUUM

directions studied. The terbium concentration N_{Tb} was estimated to be 19.6×10^{20} cm^{-3} using the measured volumetric crystal density of 4 g/cm^3. The concentration of Mo^{3+} ions, revealed in the absorption spectrum (Fig. 3) is below then the detection limits of energy dispersive spectrometer (~0.3-0.5 wt.%).

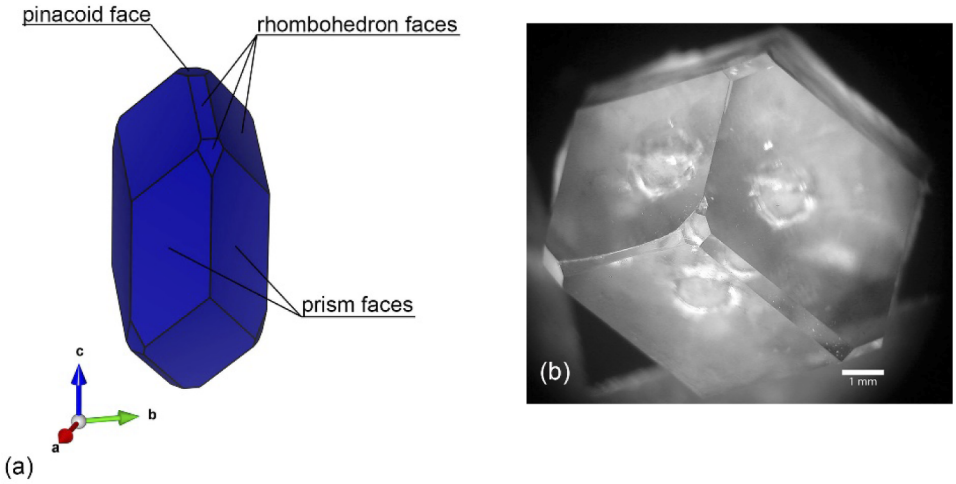

Fig. 1. (a) the growth habit of Tb:$YAl_3(BO_3)_4$ crystal (visualization: VESTA [16]) and (b) the image of crystal head

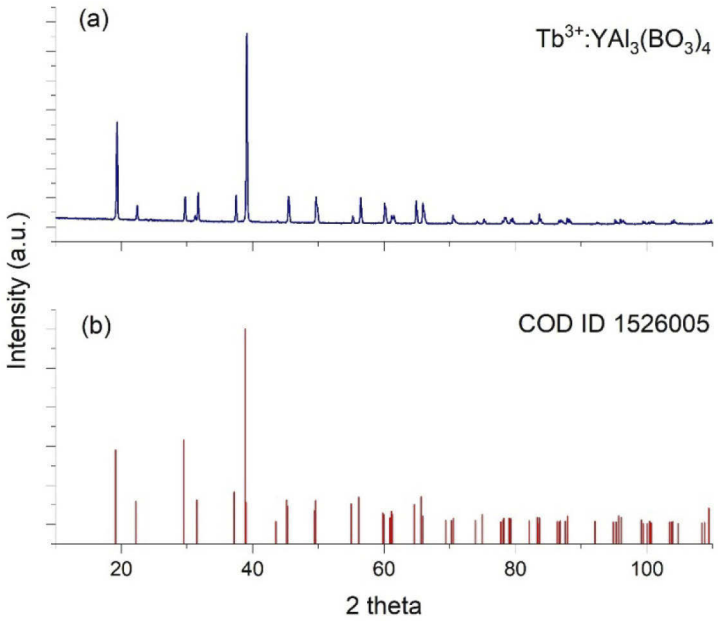

Fig. 2. XRPD patterns of (a) Tb:$YAl_3(BO_3)_4$ crystal and (b) calculated from $YAl_3(BO_3)_4$ cif-file (Crystallography open database ID 1526005)

OSA CONTINUUM

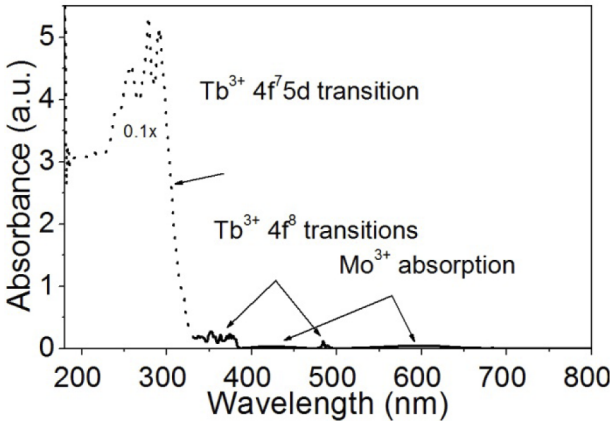

Fig. 3. Unpolarized absorption spectrum of Tb:YAB

3.1. *Ground state absorption and f-f transition intensities*

The polarization dependent ground state absorption spectra of the Tb:YAB were recorded in the 310-500 nm and 1500-2700 nm spectral ranges. The spectra were corrected for the Fresnel losses using the Sellmeier`s coefficients for the YAB crystal [17]. The spectra of absorption cross section σ_{GSA} in the UV, visible and NIR spectral ranges are shown in Fig. 4.

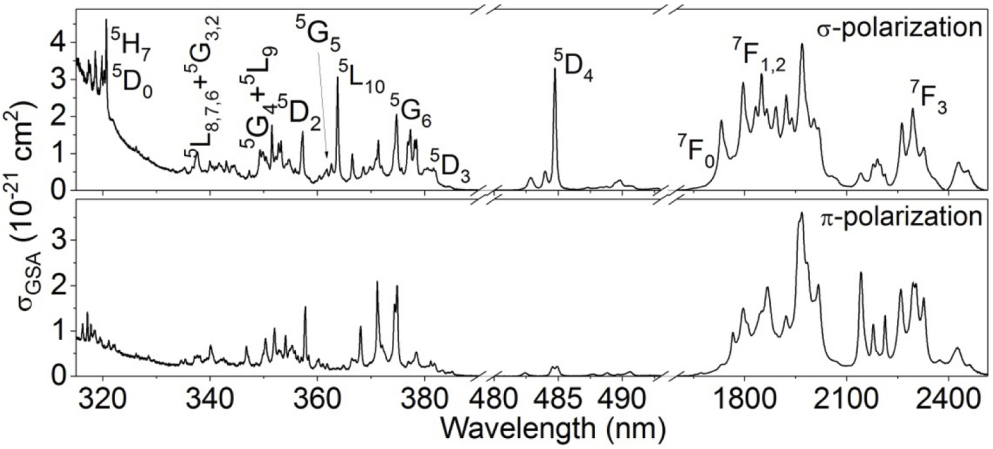

Fig. 4. Polarized ground absorption cross sections of Tb:YAB

The absorption spectra of the Tb:YAB exhibit pronounced polarization anisotropy. In the visible spectral range, the characteristic $^7F_6 \rightarrow {}^5D_4$ transition has a peak value of 3.2×10^{-21} cm^2 (for σ-polarization) at 484.7 nm that make this crystal suitable for frequency doubled optically pumped semiconductor laser or laser diode pumping in the cyan spectral region. The peak absorption coefficient of 6.8 cm^{-1} for Tb(35 at.%):YAB is larger than the absorption values of Tb-doped fluoride crystals [3]. But the efficient absorption of pumping radiation requires the accurate tuning of pumping wavelength.

Efficient populating the $^5D_4$ level is possible via the cross-relaxation process $^5D_3 \rightarrow {}^5D_4 : {}^7F_6 \rightarrow {}^7F_0$ by laser diodes pumping in the region of 370-380 nm. Despite the higher quantum defect, this spectral region possesses broader spectral lines and cross-sections values up to 2×10^{-21} cm^2.

OSA CONTINUUM

It is well known that Tb^{3+} ion among the triply ionized rare-earth ions has the lowest energetic position of the excited configuration $4f^7 5d^1$. The experimental ^9D level energy position of about 37157 cm^{-1} (Fig. 3) is in good agreement with the theoretical value of 37381 cm^{-1} based on semi-empirical method of P. Dorenbos [13]. The shortwave wing of this absorption band cannot be observed due to fundamental YAB matrix absorption with the cut-off wavelength of about 170 nm [18]. The levels of this configuration can be terminal during excited state absorption (ESA) from the upper laser level $^5D_4$. However, the interconfigurational ESA has the low probability due to the doubly spin-forbidden transitions [3]. Since the band gap energy of YAB crystals is about 7.3 eV [18], only the f-f ESA transitions can be detrimental for laser action in the visible.

The transition intensities of Tb^{3+} ions in YAB crystal were determined according to the theory of *4f-4f* transition intensities with taking into account the influence of $4f^{N-1}5d$ excited configuration. The case of intermediate configuration interaction (ICI approximation) [19] gives the best agreement between the calculated results and experimental data. The line strength S of the electric-dipole (ED) transition from initial J manifold to some terminal J' manifold, in this case, can be evaluated by the formula:

$$S_{ED,calc}(JJ') = \sum_{t=2,4,6} \Omega_t [1 + 2R_t(E_J + E_{J'} - 2E_f^0)] \cdot \left| \left\langle 4f^n[SL]J || U^{(t)} || 4f^n[S'L']J' \right\rangle \right|^2. \quad (1)$$

Here E_J and $E_{J'}$ are the energies of the multiplets involved in the considered transition, $E^0{}_f$ is the average energy of $4f^N$ configuration and R_t are additional parameters related to the configuration interaction. The squared reduced-matrix elements $||U^{(t)}||$ were calculated from the intermediate coupling approximation [20] using the free-ion parameters for the trivalent terbium ion [21]. Obtained values of $||U^{(t)}||$ are presented in Table 1.

The experimental oscillator strengths f_{exp} were calculated from the measured absorption spectra:

$$f_{\exp}(JJ') = \frac{mc^2}{\pi e^2 N_0 \bar{\lambda}^2} \int \frac{\alpha^{\pi}_{JJ'}(\lambda) + 2\alpha^{\sigma}_{JJ'}(\lambda)}{3} d\lambda. \quad (2)$$

Here $\bar{\lambda}$ is the weighted mean wavelength. The contributions of the magnetic dipole (MD) transition following the selection rule $\Delta J = 0, \pm 1$ were taken into $f_{ED,\,exp}$ through a subtraction of f_{MD} from f_{exp}. The values of f_{MD} were calculated separately within the Russell-Saunders approximation on wavefunctions of Tb^{3+} ion under the assumption of a free-ion. The values of the experimental and the calculated ED absorption oscillator strengths $f_{ED,exp}$ and f_{ED}, respectively, as well as the calculated MD oscillator strengths f_{MD} are given in Table 2.

The intensity parameters Ω_t as well as the R_t parameters were evaluated by the least-square fitting procedure and are presented in Table 3. The root mean square deviation was 0.06×10^6.

With obtained data, the radiative lifetime τ_{rad} of the $^5D_4$ and the branching ratios β can be evaluated [19]. The radiative lifetime of the $^5D_0$ state is calculated to be 1.83 ms and the calculated transitions probabilities $A_{\sum} = A_{ED} + A_{MD}$, as well as branching ratios, are listed Table 4.

3.2. Radiative properties

Polarized fluorescence spectra of Tb:YAB in the range of 475-700 nm were recorded under excitation at 488 nm and corrected to the spectral response of the luminescence set-up. The observed emission bands are related to the radiative transitions from $^5D_4$ manifold to the lower lying levels. Manifold to manifold branching ratios $\beta_{J'J}$ for the transitions from the upper state $^5D_4$ to the lower lying states are found from $\beta_{J'J} = \int \lambda I_{J'J}(\lambda) d\lambda \,/\, \sum_J \int \lambda I_{J'J}(\lambda) d\lambda$, where $I_{J'J}(\lambda)$ is the spectral density fluorescence power in arbitrary units. The experimental averaged values of $\beta_{J'J}$ over two polarizations with respect to calculated ones are presented in Table 4. It is evident

OSA CONTINUUM

Table 1. Squared matrix-elements $||U^{(2,4,6)}||$ for the J →J′ transitions of Tb^{3+} ions

SLJ	*S′L′J′*	$\|\|U^{(2)}\|\|$	$\|\|U^{(4)}\|\|$	$\|\|U^{(6)}\|\|$
$^7F_6$	$^7F_5$	0.5374	0.6419	0.1174
	$^7F_4$	0.0901	0.5158	0.2653
	$^7F_3$	0	0.2323	0.4125
	$^7F_2$	0	0.0481	0.4695
	$^7F_1$	0	0	0.3763
	$^7F_0$	0	0	0.1442
	$^5D_4$	0.0021	0.0008	0.0013
	$^5D_3$	0	0.0002	0.0014
	$^5G_6$	0.0023	0.0045	0.0119
	$^5L_{10}$	0	0.0003	0.0596
	$^5G_5$	0.0016	0.0018	0.0136
	$^5D_2$	0	0	0.0008
	$^5G_4$	0.0002	0.0003	0.0091
	$^5L_9$	0	0.0021	0.0470
	$^5G_3$	0	0.0001	0.0031
	$^5L_8$	0	0.0001	0.0236
	$^5L_7$	0.0007	0.0001	0.0119
	$^5G_2$	0	0	0.0005
	$^5L_6$	0.0001	0.0001	0.0003
$^5D_4$	$^7F_5$	0.0153	0.0014	0.0022
	$^7F_4$	0.0003	0.0022	0.0013
	$^7F_3$	0.0023	0.0005	0.0006
	$^7F_2$	0.0011	0.0004	0.0001
	$^7F_1$	0	0.0025	0
	$^7F_0$	0	0.0017	0

Table 2. Experimental ($f_{ED,\ exp}$) and calculated ($f_{ED,MD}$) oscillator strength

Transition	E, cm^{-1}	$f_{ED,\ exp}\times10^{-6}$	$f_{ED}\times10^{-6}$	$f_{MD}\times10^{-6}$
$^7F_6 \rightarrow {}^7F_3$	4371	0.432	0.427	
$^7F_6 \rightarrow {}^7F_{2,\ 1,\ 0}$	5332	1.625	1.622	
$^7F_6 \rightarrow {}^5D_4$	20570	0.078	0.059	
$^7F_6 \rightarrow {}^5D_3, {}^5G_6$	26358	0.322	0.360	0.09
$^7F_6 \rightarrow {}^5L_{10}$	26968	0.342	0.343	
$^7F_6 \rightarrow {}^5G_5$	27615	0.154	0.179	0.006
$^7F_6 \rightarrow {}^5D_2, {}^5G_4, {}^5L_9$	28300	0.482	0.415	
$^7F_6 \rightarrow {}^5G_{3,2}, {}^5L_{8,7,6}$	29372	0.194	0.257	0.002

Table 3. Fit parameters of ICI theory

Set of parameters	
Ω_t (10^{-20} cm)	$\Omega_2 = 6.925$, $\Omega_4 = 5.776$, $\Omega_6 = 1.801$
R_t (10^{-4}cm)	$R_2 = -0.166$, $R_4 = 0.382$, $R_6 = -0.115$

OSA CONTINUUM

Table 4. The calculated radiative probabilities (A_Σ), fluorescence branching ratios (β) in Tb:YAB crystal

Transition $^5D_4$ →	$\overline{\lambda}$ (nm)	A_Σ (ICI) (s^{-1})	β_{calc} (ICI)	$\beta_{J'J}$
$^7F_6$	489	62.49	13.4	13.7
$^7F_5$	545	261.15^{ED}+69.86^{MD}	60.5	61
$^7F_4$	588	40.48^{ED}+0.27^{MD}	7.5	9.6
$^7F_3$	620	30.7^{ED}+8.48^{MD}	7.2	9.4
$^7F_2$	650			1.7
$^7F_1$	668	73.41	11.4	1.1
$^7F_0$	683			3.5

that almost 60% of emitted energy is distributed in the green spectral range.

$$\sigma_{SE}^{\alpha}(\lambda) = \beta_{J'J}\frac{\lambda^5}{8\pi c n^2 \tau_{rad}}\frac{3I^{\alpha}(\lambda)}{\int [I^{\pi}(\lambda) + 2I^{\sigma}(\lambda)]\lambda d\lambda}. \quad (3)$$

Here $I^{\alpha}(\lambda)$ is the spectral density of fluorescence power (α =σ, π polarizations), τ_{rad} is the radiative lifetime of the $^5D_4$ level, $\beta_{J'J}$ is the experimental branching ratio of the corresponding transition. The obtained SE-spectra are displayed in Fig. 5. The highest cross section was found to be 3.4×10^{-21} cm^2 (λ = 541 nm) for σ polarization.

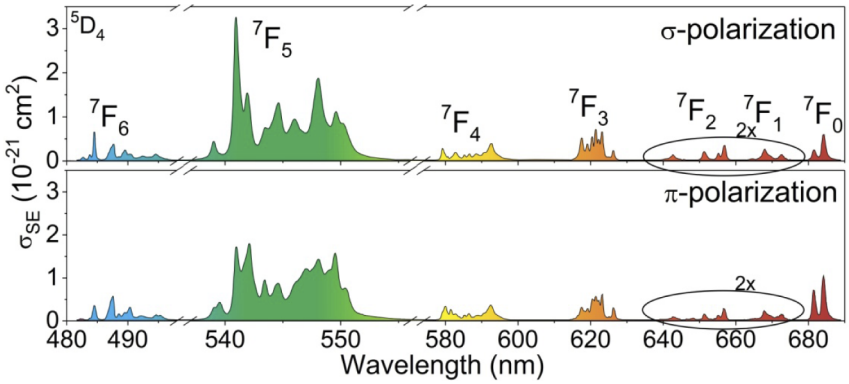

Fig. 5. Stimulated emission cross sections spectra of Tb:YAB crystal

The fluorescence lifetime of the $^5D_4$ manifold was measured at a wavelength of 545 nm under excitation at 488 nm. The obtained curve (Fig. 6(a)) is single exponential with the lifetime of 1.7 ms which is close to the radiative lifetime of the $^5D_4$ manifold (1.83 ms) calculated from the Judd-Ofelt theory. Comparison of the experimental fluorescence lifetime to the calculated radiative lifetime yields the quantum efficiency of about 93%. Figure 3 shows also the decay curve of $TbAl_3(BO_3)_4$ (TbAB). The lifetime of $^5D_4$ level is decreased up to 0.9 ms for this crystal and corresponding fluorescence quantum yield η of 49%. The fluorescence quenching is observed with increasing Tb ions concentration due to the energy transfer from Tb^{3+} ions to Mo^{3+} ions. For these cases, the decay curves are single exponential. It means, that the energy migration among Tb ions prevails over the $Tb^{3+} \rightarrow Mo^{3+}$ energy transfer. It necessary to utilize other solvents, for example $BaO\text{-}B_2O_3$ or $Li_2B_4O_7$ [22,23], during the crystal growth in order to avoid this detrimental process.

Under 355 nm pumping the fluorescence lifetime of the emitting $^5D_3$ level of Tb:YAB was measured at a wavelength of ~434 nm and the obtained decays curves with the fluorescence

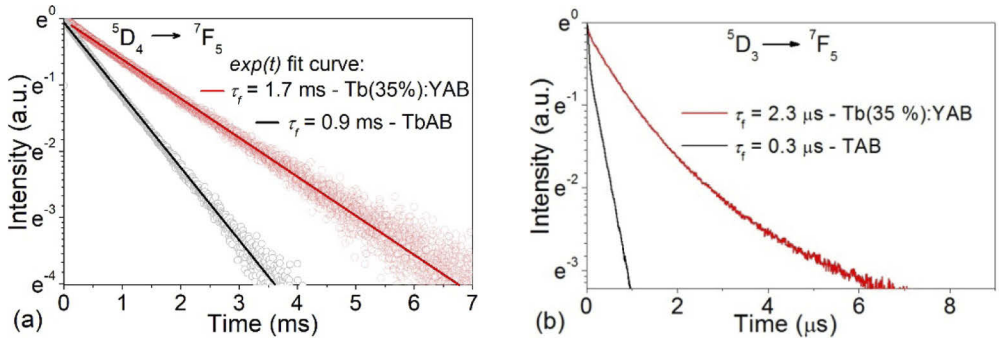

Fig. 6. Fluorescence decay curve of the $^5D_4$ (a) and $^5D_3$ (b) levels of Tb:YAB.

lifetimes are presented in Fig. 6(b). The curves have non-exponential character due to cross-relaxation process and the fluorescence lifetime was obtained from $\tau_f = \int tI(t)dt / \int I(t)dt$. The short $^5D_3$ level fluorescence lifetime and decreasing in value from 2.3μs for Tb(35% at.)YAB to 0.3μs for TbAB indicate the efficient cross-relaxation and consequently the population of $^5D_4$ level.

The obtained spectroscopic results allow to conclude, that Tb:YAB crystals are suitable candidates for laser operation in the visible spectral range. In Table 5 we compare obtained in this study spectroscopic parameters of Tb:YAB crystal with ones of other Tb-doped materials.

Table 5. Spectroscopic parameters of Tb-doped crystals

Crystal	N_{Tb} (10^{20} cm^{-3})	$\lambda_{abs,\,peak}$, (nm)	σ_{abs}, (10^{-22} cm^2)	$\lambda_{em,\,peak}$, (nm)	σ_{SE}, (10^{-22} cm^2)	τ_{rad}, (ms)	τ_{meas}, (ms)	Refs.
Tb:YAB	20.6	484.7	32	541	34	1.83	1.7	This study
Tb:$LiLiF_4$	20	488.8	3 (E||**c**)	544	16 (E||**a**)	-	4.8	[3]
Tb:$YAlO_3$	14.1	484	5.2 (E||**b**)	544	11.2 (E||**c**)	2.31	1.72	[6]
Tb:$KY(WO_4)_2$	31.8	486.7	53 (E||N_m)	549.3	90 (E||N_m)	0.47	0.35	[8]
$Ba_3Tb(PO_4)_3$	34.9	485	0.96	549.6	5.9	3.54	3.17	[9]
Tb:$Y_3Al_5O_{12}$	10.5	486	2.5	549	12.3	3.3	3.1	[24]
$SrTb(BO_3)_3$	–	~ 485	1.1	543	5.6	3.1	3	
$Li_6Tb(BO_3)_3$	–	~ 485	2.8	543	11	2.9	2.6	[25]
$TbCa_4O(BO_3)_3$	–	~ 485	5.4	553	12	3.2	3.1	

4. Conclusion

A high quality single crystal of Tb^{3+}-doped $YAl_3(BO_3)_4$ was grown by dipping seeded high-temperature solution growth method. The most suitable pumping transition $^7F_6 \rightarrow {}^5D_4$ has a peak absorption cross section of 3.2×10^{-21} cm^2 (for σ-polarization) at a wavelength of 487.7 nm. However, the spectral region of 370-380 nm with absorption cross section values up to 2×10^{-21} cm^2 can be used for laser diode pumping. The highest stimulated emission cross sections of 3.4×10^{-21} cm^2 (for σ- polarization) was found in the green spectral region at 541 nm. The 4f-4f transition intensities were calculated by applying the theory for a system with intermediate configuration interaction and the radiative lifetime of the upper state $^5D_4$ was derived to be about 1.95 ms. The fluorescence lifetime and quantum efficiency of this level were found to be 1.7 ms and 87%, respectively for terbium ion concentration of 35 at. %. High values of cross-section

OSA CONTINUUM

in the absorption and luminescence with the low value of the crystal field depression make Tb^{3+}-doped YAB crystals suitable for visible laser operation in the green spectral range.

Funding. Russian Foundation for Basic Research (18-29-12091mk).

Acknowledgment. M. Demesh appreciates BRFFR (F20MB-10) for the partial support of this research.

Disclosures. The authors declare no conflicts of interest.

References

1. G.P. Agraval, *Lightwave technology: Component and devices* (John Willey & Sons, 2004).
2. M. Nazarov and D.Y. Noh, *New generation of terbium- and europium- activated phosphors: from syntheses to applications* (Pan Stanford publishing, 2011).
3. P. W. Metz, D.-T. Marzahl, A. Majid, C. Kränkel, and G. Huber, "Efficient continuous wave laser operation of Tb^{3+}-doped fluoride crystals in the green and yellow spectral regions," Laser Photonics Rev. **10**(2), 335–344 (2016).
4. E. Castellano-Hernández, P. W. Metz, M. Demesh, and C. Kränkel, "Efficient directly emitting high-power Tb^{3+}:$LiLuF_4$ laser operating at 587.5 nm in the yellow range," Opt. Lett. **43**(19), 4791–4794 (2018).
5. E. Castellano-Hernandez, S. Kalusniak, P. W. Metz, and C. Kränkel, "Diode-Pumped Laser Operation of Tb^{3+}:$LiLuF_4$ in the Green and Yellow Spectral Range," Laser Photonics Rev. **14**(2), 1900229 (2020).
6. B. Liu, J. Shi, Q. Wang, H. Tang, J. Liu, H. Zhao, D. Li, J. Liu, X. Xu, Z. Wang, and J. Xu, "Crystal growth, polarized spectroscopy and Judd-Ofelt analysis of Tb:$YAlO_3$," Spectrochim. Acta, Part A **200**, 58–62 (2018).
7. P. Loiko, A. Volokitina, X. Mateos, E. Dunina, A. Kornienko, E. Vilejshikova, M. Aguilo, and F. Díaz, "Spectroscopy of Tb^{3+} ions in monoclinic $KLu(WO_4)_2$ crystal application of an intermediate configuration interaction theory," Opt. Mater. **78**, 495–501 (2018).
8. M. Demesh, A. Mudryi, A. Pavlyuk, E. Castellano-Hernández, C. Kränkel, and N. Kuleshov, "Cross sections and transition intensities of Tb^{3+} in $KY(WO_4)_2$," OSA Continuum **2**(4), 1378–1385 (2019).
9. H. Chen, P. Loiseau, G. Aka, and C. Kränkel, "Optical spectroscopic investigation of $Ba_3Tb(PO_4)_3$ single crystals for visible laser applications," J. Alloys Compd. **740**, 1133–1139 (2018).
10. N. Ben Amar, M. A. Hassairi, and M. Dammak, "Optical spectroscopy and crystal field calculation of Tb^{3+} doped in $YAl_3(BO_3)_4$ single crystal," J. Lumin. **173**, 223–230 (2016).
11. I. Couwenberg, K. Binnemans, H. De Leebeeck, and C. Gorller-Walrand, "Spectroscopic properties of the trivalent terbium ion in the huntite matrix $TbAl_3(BO_3)_4$," J. Alloys Compd. **274**(1-2), 157–163 (1998).
12. S. Colak and W. K. Zwicker, "Transition rates of Tb^{3+} in TbP_5O_{14}, $TbLiP_4O_{12}$, and $TbAl_3(BO_3)_4$: An evaluation for laser applications"," J. Appl. Phys. **54**(5), 2156–2166 (1983).
13. P. Dorenbos, "The 5d level positions of the trivalent lanthanides in inorganic compounds," J. Lumin. **91**(3-4), 155–176 (2000).
14. V. V. Maltsev, E. A. Volkova, N. I. Leonyuk, N. A. Tolstik, and N. V. Kuleshov, "Highly efficient Er- and Yb-doped $YAl_3(BO_3)_4$ laser materials: crystal growth and characterization," J. Opt. Adv. Mater. **10**(11), 2890–2893 (2008).
15. T. J. B. Holland and S. A. T. Redfern, "Unit cell refinement from powder diffraction data: the use of regression diagnostics," Mineral. Mag. **61**(404), 65–77 (1997).
16. K. Momma and F. Izumi, "VESTA 3for three-dimensional visualization of crystal, volumetric and morphology data," J. Appl. Crystallogr. **44**(6), 1272–1276 (2011).
17. R. Martinez Vazquez, R. Osellame, M. Marangoni, R. Ramponi, and E. Dieguez, "Er^{3+} doped $YAl_3(BO_3)_4$ single crystals: determination of the refractive indices," Opt. Mater. **26**(3), 231–233 (2004).
18. X. Yu, Y. Yue, J. Yao, and Z. Hu, "$YAl_3(BO_3)_4$: Crystal growth and characterization," J. Cryst. Growth **312**(20), 3029–3033 (2010).
19. E. B. Dunina and A. A. Kornienko, "Influence of excited configurations on the intensities of electric-dipole transitions of rare-earth ions," Opt. Spectrosc. **116**(5), 706–711 (2014).
20. B.G. Wybourne, *Spectroscopic properties of rare earths* (Wiley, New York, 1965).
21. I. D. Morrison, A. J. Berry, and R. G. Denning, "Energy levels of terbium(III) in the elpasolite $Cs_2NaTbCl_6$," Mol. Phys. **96**(1), 43–51 (1999).
22. S. A. Payne, L. L. Chase, L. K. Smith, W. L. Kway, and W. F. Krupke, "Infrared cross-section measurements for crystals doped with Er^{3+}, Tm^{3+}, and Ho^{3+}," IEEE J. Quantum Electron. **28**(11), 2619–2630 (1992).
23. E. Cavalli and N. I. Leonyuk, "Comparative Investigation on the Emission Properties of $RAl_3(BO_3)_4$ (R = Pr, Eu, Tb, Dy, Tm, Yb) Crystals with the Huntite Structure," Crystals **9**(1), 44 (2019).
24. J. Liu, Q. Song, D. Li, Y. Ding, X. Xu, and J. Xu, "Spectroscopic properties of Tb:$Y_3Al_5O_{12}$ crystal for visible laser application," Opt. Mater. **106**, 110001 (2020).
25. H. Chen, P. Loiseau, G. Aka, B. Baptiste, and P. Veber, "Crystal growth and characterization of terbium-based borate crystals of $Sr_3Tb(BO_3)_3$, $Li_6Tb(BO_3)_3$, and $TbCa_4O(BO_3)_3$: color centers, spectroscopic properties, and optical gain," Cryst. Growth Des. **20**(3), 1905–1919 (2020).